

## **Association between congenital defects in papillary outgrowth and functional obstruction in *Crim1* mutant mice.**

Lorine Wilkinson<sup>1</sup>, Nyoman D Kurniawan<sup>2#</sup>, Yu Leng Phua<sup>1#</sup>, ~~Joan Li<sup>1</sup>~~, Michael Nguyen<sup>3</sup>, Graham J Galloway<sup>2</sup>, Hikaru Hashitani<sup>4</sup>, Richard Lang<sup>3</sup>, Melissa H. Little<sup>1\*</sup>.

<sup>1</sup>Institute for Molecular Bioscience, The University of Queensland, QLD 4072, Australia

<sup>2</sup>Centre for Advanced Imaging, The University of Queensland, QLD 4072, Australia

<sup>3</sup>Department of Physiology, School of Biomedical Sciences, Monash University, VIC 3800, Australia.

<sup>4</sup>Nagoya City University, Japan

# These authors contributed equally to this study.

\*Corresponding author:

Professor Melissa H Little

NHMRC Principal Research Fellow

Institute for Molecular Bioscience

The University of Queensland

St. Lucia, 4072

Australia

Ph: +61 7 3346 2054

FAX: +61 7 3346 2101

email: M.Little@imb.uq.edu.au

**Keywords:** obstructive nephropathy, functional obstruction, hydronephrosis, magnetic resonance imaging, Crim1, pyeloureteric peristalsis

The authors have declared no conflicts of interest exist.

## Abstract

Crim1 hypomorphic ( $\text{Crim1}^{\text{KST264/KST264}}$ ) mice display progressive renal disease characterised by glomerular defects, leaky peritubular vasculature and progressive interstitial fibrosis. Here we show that 27% of these mice also present with hydronephrosis, suggesting obstructive nephropathy. Using magnetic resonance imaging, T<sub>2</sub>-weighted hypointense staining was observed in the kidneys of  $\text{Crim1}^{\text{KST264/KST264}}$  mice suggesting pooling of filtrate within the renal parenchyma. Rhodamine dextran (10kD) clearance was also delayed in  $\text{Crim1}^{\text{KST264/KST264}}$  mice. Pyeloureteric peristalsis, while present, was less coordinated in  $\text{Crim1}^{\text{KST264/KST264}}$  mice and electrophysiological studies of isolated ureter/pelvis identified a reduced frequency of smooth muscle contraction, despite evidence for pacemaker activity. An analysis of maturation during the immediate postnatal period (postnatal day (P)0-20) revealed marked defects in papillary extension in  $\text{Crim1}^{\text{KST264/KST264}}$  mice. Crim1 expression was observed in pelvic smooth muscle and strongly in the interstitium and loops of Henle of the extending papilla, commencing at the tip and disseminating throughout the papilla by P10. These results, as well as implicating Crim1 in papillary extension and pelvic smooth muscle contractility, highlights the previously unrecognised association between defects in papillary development and progression to chronic kidney disease later in life.

(183 words)

## Introduction

Congenital anomalies of the kidney and urinary tract (CAKUT) occur in 1 in 500 humans, constituting approximately 20-30% of all anomalies identified in the prenatal period ~~(Winyard and Chitty, 2008; Schedl)~~<sup>1,2</sup> CAKUT encompasses a wide array of defects, including agenesis (no kidney), hypoplasia (small kidney) and dysplastic anomalies including duplicated collecting systems, duplex kidneys and megaureter, occurring alone or as part of multi-organ syndromes. One of the most frequent presentations in CAKUT is obstructive nephropathy, found in 1 in 1000 live births and representing the most common cause of renal failure in children ~~(Klein)~~<sup>3</sup> Here nephropathy is caused by an obstruction at either the junction of the ureter and bladder (uretero vesicular junction (UVJ)) or the junction of the ureter and pelvis (uretero pelvic junction (UPJ)). Such obstructions may result from a 'physical' blockage ~~or stricture~~ of the ureter, urethra or bladder ~~(e.g. megaureter, secondary VUR)~~ or represent 'functional' obstruction, where a more subtle developmental defect ~~in the formation of the collecting ducts, pelvis or ureter~~ results in impaired urine flow.

~~Exit of the urinary filtrate from the kidney requires not only the presence of a conduit but the appropriate formation and differentiation of a watertight pelvis, ureteropelvic junction, ureter invested with contractile smooth muscle and a pacemaker driving productive contractions.~~

Urine is cleared from the pelvis of the mature kidney due to the spontaneous propagating contractions of a layer of typical smooth muscle cells (tSMC) lining the pelvis itself.<sup>ref</sup> As this layer is contiguous with the smooth muscle of the ureter, such peristaltic waves move the filtrate from the pelvis along the ureter to the

Formatted: Superscript

Formatted: Superscript

Formatted: Font color: Red, Superscript

bladder. This process is called pyeloureteric peristalsis. Electrophysiological studies have shown that propagation of contractions across this tSMC layer result from transient rises in intracellular Ca<sup>2+</sup> concentration entering the cell via L-type voltage operated calcium channels that open during the action potential.<sup>Lang</sup> ~~(Lang?)~~. It has long been accepted that these contractions are initiated by pacemaker cells deep within the kidney, however the identity and location of this pacemaker remains controversial ~~(Gosling and Dixon, 1974, Lang et al, 2010)~~.<sup>Golsing, Lang</sup> Productive clearance of urinary filtrate is ~~presumably~~ facilitated by the fact that pyeloureteric peristalsis is initiated at the pelvis-kidney junction (PKJ), with pacemaker cells present in this location at the base of the papilla. The resulting coordinated contractile wave squeezes the papilla, effectively 'milking' the urinary filtrate from the collecting ducts via constriction of this region ~~(Dwyer and Schmidt-Neilsen, 2003)~~.<sup>Dwyer, Hurtado</sup> Presumably, ~~therefore~~, loss of pacemaker cells, loss of tSMC contractility, loss of correct tSMC investment of the pelvis or disruptions to the coordinated progressive of the peristaltic wave would all ~~be anticipated to~~ result in functional obstruction and hydronephrosis.

Formatted: Font color: Red, Superscript

Formatted: Font color: Red, Superscript

Formatted: Font color: Red, Superscript

-The activity of most growth factors is modulated both positively and negatively via co-receptors, secreted inhibitors and regulators of processing and secretion. One such modulator is Crim1. The transmembrane protein Crim1 ~~has previously been reported to~~ plays a critical role in the regulation of VEGF signalling in the developing glomerulus ~~due to via the a loss of appropriate Vegfa tethering of Vegfa at to the surface of the~~ podocytes ~~(Wilkinson et al 2007)~~.<sup>Wilk07</sup> On an inbred background, the loss of Crim1 leads to simplified glomerular capillary development and podocyte effacement ~~(Wilkinson et al 2007)~~.<sup>Wilk07</sup> Postnatal outbred Crim1 hypomorphic mice

Formatted: Indent: First line: 0 cm, Don't adjust space between Latin and Asian text

Formatted: Font color: Red, Superscript

(Crim1<sup>KST264/KST264</sup>) also show podocyte effacement together with proteinuria, glomerular cysts and reduced GFR, all of which are likely to be caused by disruptions to Crim1 in the podocytes ~~(Wilkinson et al, 2007).~~<sup>Wilk07</sup> However, they also display a loss of vascular integrity and progressive renal fibrosis.<sup>Wilk09</sup> ~~-(Wilkinson et al, 2009).~~ Growth factor binding by Crim1 is not restricted to Vegfa. Crim1 is also capable of tethering at the cell surface other cystine-knot containing growth factors, including Pdgf, Bmp and Tgf proteins ~~(Wilkinson et al, 2003).~~<sup>Wilk03</sup> In this way, loss Crim1 from specific cell types ~~is likely to may~~ perturb a number of growth factor signalling pathways, with the specific site of Crim1 expression dictating the growth factor signalling pathways affected.

In this study, we report the presence of hydronephrosis in a proportion of Crim1<sup>KST264/KST264</sup> mice, revealing evidence for underlying functional obstruction in these mice even in the absence of hydronephrosis. ~~As-While~~ pacemaker cell activity is present and the pelvic tSMC layer is contractile, ~~there is evidence for less productive waves of peristalsis occurring at a lower frequency than observed in wildtype animal~~ ~~these mice show defects in the extension of the papilla during the immediate postnatal period. This significant reduction in papillary length is likely to reduce the area of collecting duct being exposed to peristaltic contraction. This defect coincides with the onset of Crim1 expression~~ ~~Expression of Crim1 within the interstitium of the papilla. appears from birth and increases during the period of postnatal papillary maturation and extension. An analysis of this process revealed a significant reduction in papillary length in Crim1<sup>KST264/KST264</sup> mice, with this likely to result in a smaller are of collecting duct being exposed to peristaltic contraction.~~ We therefore propose that the obstructive phenotype, and hence the resultant progressive renal fibrosis, results both

from an underlying failure of the renal papilla to appropriately extend from the body of the kidney ~~during the first two weeks of life coupled with anomalies in propagation of peristalsis~~. These observations have implications not only for our understanding of functional obstruction but also ~~associate-link~~ papillary ~~anatomy-extension~~ with long term renal function, a potentially underappreciated and undocumented causative agent in chronic kidney disease.

## Results

**Crim1<sup>KST264/KST264</sup> adult mice show ~~loss of corticomedullary differentiation and partially penetrant hydronephrosis.~~**

As well as glomerular pathology, we have previously reported that Crim1<sup>KST264/KST264</sup> mice develop progressive renal disease characterised by interstitial fibrosis (Wilkinson et al, 2009). To further investigate the progression of disease, temporal MRI was performed on adult wild-type and Crim1<sup>KST264/KST264</sup> mice. Anatomical scans were performed on anaesthetised mice using a fast spin echo T<sub>2</sub>-weighted fast spin echo (RARE) sequence. ~~Contiguous 0.8 mm slices of entire kidneys were acquired. Image acquisition, and therefore resolution, was more problematic for Crim1<sup>KST264/KST264</sup> mice due to respiration irregularities.~~ Images of wildtype kidneys showed clear corticomedullary differentiation (CMD) (Figure 1AB), in contrast to Crim1<sup>KST264/KST264</sup> kidneys (Figure 1CD). Loss of appropriate CMD is correlated with degree of renal function and is eventually lost in renal failure ~~(Grenier N 2006)~~<sup>Grenier</sup>. As previously reported, prominent cysts were seen in Crim1<sup>KST264/KST264</sup> mice<sup>ref</sup>. In addition, frank hydronephrosis was present in 3/8 imaged Crim1<sup>KST264/KST264</sup> mice. Imaging performed on the same animals over time revealed a progressive onset of hydronephrosis (Figure 2A). After reanalysis of histological sections across a larger cohort of Crim1<sup>KST264/KST264</sup> mice ~~aged from~~ (-8-28 wks of age), the prevalence of hydronephrosis was found to be 27% (n=22). Features observed included enlarged pelvis and atrophied papillae (Figure 2B). TUNEL staining revealed apoptotic cells lining the pelvis in these mice (Figure 2C).

**Assessment of functional obstruction using dynamic contrast-enhanced MRI.**

Formatted: Font color: Red, Superscript

Formatted: Font color: Red, Superscript

The presence of hydronephrosis suggested a urinary outflow obstruction. Dynamic contrast enhanced (DCE) MRI was used to investigate this further. Magnevist® (Bayer), a gadolinium containing contrast agent (gadolinium diethylenetriamine pentaacetic acid (Gd-DTPA)) was used as an intravenously administered contrast agent. ~~The small molecular weight (<1kDa) and biochemical properties of Gd-DTPA enables rapid distribution throughout all tissues other than the central nervous system, where the blood brain barrier is impermeable to this molecule. The volume of distribution in the tissues is equivalent to that of extracellular water and in humans the distribution half-life is approximately 4 minutes (Abraham JL 2008).~~ In the kidneys, Gd-DTPA is filtered by the glomerulus and neither secreted or reabsorbed by the tubules ~~(Choyke et al, 2005).~~ <sup>Choyke</sup> The elimination half-life for gadolinium contrast agents from the human kidney is approximately 70 minutes with 85% cleared within 4 hours ~~(Abraham JL 2008).~~ <sup>Abraham</sup> At low concentrations, Gd-DTPA shows hyperintensity (bright) under a T1-weighted image. However at higher concentrations, the shortening of T<sub>2</sub> effects become predominant and images become hypointense (dark).

Three sibling pairs, consisting of a wild-type and Crim1<sup>KST264/KST264</sup> mouse ~~(7-8 weeks of age)aged between 7 and 8 weeks,~~ were imaged using DCE-MRI. An image baseline was acquired prior to administration of Gd-DTPA (0.1-0.15 mmol/kg body weight). ~~Each mouse was imaged~~ immediately after injection and then again at approximately 15 minute intervals for ~~approximately 2 hours~~ up to 19 hours. A temporal series of images of one such wildtype / Crim1<sup>KST264/KST264</sup> sibling pair are shown in Figure 3AB. Immediately after injection there was a dramatic increase in signal intensity in wild-type mice, indicating rapid systemic Gd-DTPA diffusion (Figure 3A). From 10 to 35 minutes, contrast agent concentrated in the medulla of the kidney with the resulting

**Formatted:** Font: Font color: Red, English (U.S.), Superscript

increase in Gd-DTPA resulting in a T<sub>2</sub> effect (hypointensity) ~~in the concentrated urine~~ (Figure 3A). As Gd-DTPA was then eliminated from the kidney via the ureter, the T1 effect recovered and the papilla returned to baseline intensity, as did the remainder of the kidney. Time-signal intensities show that whole kidney intensity peaked within the first 10 minutes, ~~and~~ dropped to 50% ~~of baseline~~ at 48 minutes and 5% at 140 minutes (Figure 3C). In contrast, strong hypointensity of Gd-DTPA across all compartments of the Crim1<sup>KST264/KST264</sup> kidney was observed as soon as Gd-DTPA was introduced (Figure 3B) with signal intensity falling below baseline within 10 minutes and continuing to decrease for the period of imaging (Figure 3C). Gd-DTPA accumulation was still evident after 19 hours (Figure 3B). These MRI studies showed evidence for delayed clearance of urinary filtrate in all mice examined despite the absence of hydronephrosis, hydroureter or any evidence for a physical ureteric obstruction. ~~Indeed, imaging showed~~ contrast agent reached the bladder of Crim1<sup>KST264/KST264</sup> mice, discounting a physical block in passage of urine to the bladder.

To confirm Gd-DTPA accumulation in the kidney occurred due to reduced urinary filtrate clearance rather than the leaky peritubular vasculature previously reported in this genotype,<sup>Wilk09</sup> DCE MRI was performed on wild-type mice subjected to either unilateral ureteral obstruction (UUO) for 24 hours<sup>Cochrane</sup> or unilateral renal ischemia due to 50 minutes of renal artery clamping followed by reperfusion (IRI)<sup>Vergheze</sup> (Supplementary Figure 1).

**Gd-DTPA accumulation is seen in unilateral ureteric obstruction.**

To confirm Gd-DTPA accumulation and concentration in the kidney occurred as a result of reduced urinary filtrate clearance rather than the leaky peritubular vasculature previously reported in this genotype (Wilkinson et al, 2009), DCE-MRI was performed on wild-type mice subjected to either unilateral ureteral obstruction (UUO) for 24 hours (Cochrane et al, 2005) or unilateral renal ischemia due to 50 minutes of renal artery clamping followed by reperfusion (IRI) (Verghese E et al 2007). The contralateral kidney in both these models acted as an internal control and all kidneys were imaged 24 hrs after surgery. Quantitation of Magnevist clearance is shown in Figure 4C. Renal damage after 24 hrs UUO is limited to mild hydronephrosis, reduced renal blood flow and GFR (Chevalier R 2009), while injury at 24hrs post IRI results in leaky peritubular vasculature, interstitial inflammation and edema (Sutton et al 2003). Hemimounts of kidneys were harvested immediately after imaging. Mild hydronephrosis / pelvic dilation was evident in the UUO kidney (Figure 4B). Hemorrhagic congestion apparent in the medulla of the IRI kidney (Figure 4A) is typical of hypoxic injury to the medulla and is associated with localised decreases in MRI signal intensity due to the paramagnetic characteristics of the iron within the hemoglobin (Grenier N 2006). DCE imaging of the contralateral kidneys for both damage models showed results consistent with a normal kidney. While hypointensity did not occur in any region of the IRI kidney (Figure 4A), hypointensity was evident throughout the UUO kidney within 30 minutes of Magnevist injection and remained for the duration of imaging (Figure 4B). Hence, obstruction does indeed result in widespread hypointense staining.

**Accumulation of tubular rhodamine dextran indicates obstruction at the level of collecting duct.**

To examine this further, clearance of rhodamine dextran (RD, 10kD) at 40 minutes post tail vein injection was examined in *Crim1*<sup>KST264/KST264</sup> and wild-type mice. This small molecular weight molecule readily passes through the GBM into the urine, as was evident by the presence of RD in the urine of both WT and *Crim1*<sup>KST264/KST264</sup> mice at point of euthanasia. Fresh kidney hemimounts showed retention of RD throughout the kidney in *Crim1*<sup>KST264/KST264</sup> mice ~~with some particularly bright areas evident~~ (Figure 45C,D). This was not present in wild-type kidneys (Figure 45A,B). Thin cryosections of wild-type mice showed little RD within the kidney, however in *Crim1*<sup>KST264/KST264</sup> kidneys, RD fluorescence was evident in the lumen and within the cells of papillary tubules, identified as collecting duct via co-immunolocalization with Aqp2. In contrast, there was no co-localisation of Aqp1 and RD, ~~suggesting particular delay in passage of urine through the collecting ducts~~. This data, taken together with the Magnevist clearance results, suggest functional obstruction exists in all *Crim1*<sup>KST264/KST264</sup> mice and that this precedes frank hydronephrosis or overt progressive fibrosis.

### ***Crim1*<sup>KST264/KST264</sup> adult mice show abnormal pyeloureteric peristalsis**

~~Aberrant development of the peristaltic machinery could result in functional obstruction. Considering As *Crim1* is expressed in smooth muscle of the renal pelvis (Pennisi et al, 2007), <sup>Pennisi07</sup> aberrant development of any part of the peristaltic machinery could conceivably result in functional obstruction. To investigate this possibility, ~~wewe~~ analysed movies of pyeloureteral peristaltic contractions in hemidessected kidneys (3-12 wks postnatal) as previously described (Hurtado et al, 2010). <sup>Hurtado</sup> Analysis was performed on a total of 10 non mutant and 8 kidneys from 3-12 weeks of age. Using edge detection software (Image J) ~~to examine~~, both the frequency and velocity of the spontaneous contractions ~~could be examined~~ (Figure~~

Formatted: Font: Italic

Formatted: Font color: Red, Superscript

56), n= No significant difference in peristaltic frequency was observed between the two groups (wild-type  $7.8 \pm 0.99 \text{ min}^{-1}$  (mean  $\pm$  S.E.M); mutant  $5.95 \pm 0.99 \text{ min}^{-1}$ ;  $P > 0.05$ ); however propagation of the initial contraction was abnormal in a proportion of mutant animals (Supplementary Movies ~~\*\*\* to \*\*1-4\*~~). In wild-type kidneys, peristaltic contractions initiated near the base of the papilla were circumferentially orientated and propagated distally along the longitudinal axis passing down the length of the ureter. Crim1<sup>KST264/KST264</sup> mice (n=8) displayed a shortened papilla, often creating a void in the distal renal pelvis and resulting in contractions in both the circular and longitudinal direction near synchronously with the ureter (Figure 56Bii; Supplementary Movies ~~1-4\*\*\*~~).

### Electrophysiological analyses of isolated pelvis preparations

To examine whether the observed peristaltic propagation defects arose from inherent smooth muscle pathology, the pelvic muscle wall was dissected free of the kidney ~~parenchyma~~ and the pharmacological profile examined. In both wild-type and mutant preparations, the muscle wall of the mid renal pelvis loaded with fluo-4, an indicator of intracellular  $\text{Ca}^{2+}$  concentration, displayed  $\text{Ca}^{2+}$  waves which swept across the field of view and were invariably accompanied by a muscle wall contraction (Figure 6A). This suggests no difference in the capacity of the muscle to propagate action potentials. While isolated pelvic preparations of both non-mutant (n=3) and Crim1<sup>KST264/KST264</sup> (n=3) mice displayed spontaneous propagating contractions, the mean contraction frequency ~~of contractions~~ in Crim1<sup>KST264/KST264</sup> mice ( $17 \pm 1 \text{ min}^{-1}$ ) was significantly less than non-mutant mice ( $26.7 \pm 1.5 \text{ min}^{-1}$ ;  $p < 0.05$ ; Fig 67Di). This may reflect a slight disruption to pacemaker activity or coupling. In contrast, the velocity of propagation was not significantly different ( $0.56 \pm 0.11$  and  $0.76 \pm 0.4 \text{ mm.s}^{-1}$  respectively;  $p > 0.05$ ; Fig

~~67Dii). This may reflect a slight disruption to pacemaker activity or coupling.~~ No other defects were observed that distinguished smooth muscle behaviour between the genotypes. ~~All preparations responded to 30mM KCL via a transient increase in contraction amplitude followed by a decrease frequency until a sustained contraction was observed. Renal pelvises from both mutant and non-mutant mice (Fig 67Bi,Ci). Contraction responded to 30mM KCl via a transient increase in contraction amplitude followed by a decrease frequency until a sustained contraction was observed. These effects were readily reversed upon washing. fr~~ Frequency and velocity of contraction was decreased in proportion to indomethacin concentration ~~of indomethacin administration~~ (10 and 20  $\mu$ M) (Fig 67Bii,Cii) ~~in all preparations~~ and this was reversed upon application of the stable prostaglandin F2 $\alpha$  analog, Dinoprost (10 nM) (Fig 67Biii,Ciii, Di-ii). Finally, there was no difference between mutant and non-mutant mice in their responsiveness to Dinoprost (10 nM) or the  $\alpha$ -adrenoceptor agonist, phenylephrine (1 mM), in the absence of indomethacin (data not shown). Hence, the only apparent difference in smooth muscle physiology was a subtle reduction in frequency of spontaneous contraction in mutant mice.

#### **Crim1<sup>KST264/KST264</sup> mice show hypoplastic renal papilla development.**

As papillary hypoplasia was consistently evident in mutant mice, we quantified papilla length with respect to total kidney length between wild-type and Crim1<sup>KST264/KST264</sup> mice from P0 to P15, revealing a significant reduction in the Crim1<sup>KST264/KST264</sup> mice (Figure 78A-C). While we have previously reported *Crim1* expression in the ureter and papilla ~~(Pennisi et al 2007, Wilkinson et al 2009), Wilk09, Pennisi09~~ we have not previously identified the expressing cell type/s. LacZ staining revealed *Crim1* expression in the interstitium and Loop of Henle restricted to the tip of

Formatted: Font: Font color: Red, English (U.S.), Superscript

the papilla at P0, with expression becoming stronger and more widespread during postnatal papilla development (Figure 7\*\*\*-\*\*\*8), suggesting a temporospatially appropriate potential for Crim1 to be involved in this process.

Formatted: Font: Font color: Red, English (U.S.)

## Discussion

In this study, we report a previously unrecognized functional obstructive phenotype in mice carrying a hypomorphic mutation of the *Crim1* gene ~~that appears to result from an underlying defect in the extension of the papilla that occurs during the immediate postnatal period~~. While ~~propagation of productive~~ peristalsis in *Crim1* mutant mice appeared ~~abnormal-uncoordinated~~ in whole kidney preparations, Ca imaging and electrophysiological studies of isolated pelvis indicate the presence of pacemaker cells and a contractile tSMC layer. However, ~~the the normal~~ extension of the papilla from the renal parenchyma ~~that occurs induring~~ the immediate postnatal period was significantly disrupted in *Crim1*<sup>KST264/KST264</sup> mice. These observations link the functional obstruction observed in *Crim1*<sup>KST264/KST264</sup> mice with an underlying defect in papillary maturation rather than with an inherent anomaly in the pyeloureteric machinery.

How does a shortened papilla result in functional obstruction and how is this associated with the presence of progressive renal fibrosis in this mutant mouse strain? Recent studies have identified a number of growth factor signalling pathways ~~and molecules~~ involved in differentiation and investment of the smooth muscle and establishment of the peristaltic machinery, including the Hedgehog pathway (*Shh/Ptch1*), the renin-angiotensin system and *Bmp4* signaling (refs). Defects in these pathways can result in hydronephrosis either during embryogenesis or postnatally. Interestingly, ~~the failed smooth muscle investment of the pelvis and ureter observed in models of disruption to the RAS or calcineurin in several of these models (refs please; Chang et al, 2004), the defect (refs please; Chang et al, 2004)~~ is accompanied by aberrant papillary extension, suggesting co-ordinate development of these two events. In *Crim1*<sup>KST264/KST264</sup> mice, we have been able to show that functional obstruction

develops in the presence of a contractile smooth muscle layer and pacemaker cells with the primary defect relating to papillary extension. We propose that as the papilla extends down into the exiting ureter, this creates a greater surface area subject to peristaltic contractions and therefore enhanced urinary filtrate clearance. As a shortened papilla preceded evidence of hydronephrosis and overt renal disease, we propose that ineffective urinary clearance is present early and that this results in fibrosis of the interstitium surrounding the pelvis ultimately leading to progressive renal disease.

This study shows that the elongation of the murine papilla occurs during the first two weeks of life, extending ~~as~~ as much as 2.2 mm in a 10 day period. Almost nothing is known about the mechanism regulating this process, however this must involve considerable extension of the component tubules within the papilla. Surprisingly, there is little evidence in the literature for proliferation in the medullary collecting duct cells during this timeframe (\*\*refs). We have previously proposed that the complex phenotype ~~that presents~~ ~~presenting~~ in *Crim1* hypomorphic mice ~~could is likely to~~ result from disturbances to the signalling of ~~potentially~~ many growth factors involved in kidney development, with specific anomalies linked to the cell types in which *Crim1* is being expressed and the growth factors it is regulating in that cell type (Wilkinson et al, 2007). In previous studies, ~~w~~ ~~as~~ we have demonstrated a defect in Vegfa secretion from the podocytes in these mice, resulting in glomerular defects (Wilkinson et al 2007). In the case of the papillary defect, we show here that *Crim1* expression is observed within the interstitial cells and loops of Henle of the papillary tip from birth, suggesting a role for this protein in papillary extension. Wnt signalling, through both canonical (Wnt7b) and non-canonical (Wnt9b) pathways, has been shown to regulate elongation of the loops of Henle and collecting duct (Yu et al, 2009; Karner 2010) [Pietila I et al 2011](#), [Suburi et al](#)

2008). However, these ligands are expressed within the collecting duct themselves, therefore not co-locating with Crim1. There is also no evidence for Crim1 interactions with Wnt proteins. However, Wnt7b is known to act non-cell autonomously with the response of the tubular epithelium mediated via the interstitium. Interstitial growth factors proposed to be involved include EGF and the renin angiotensin system (refs). While the specific signalling affected is not clear, we do propose that this process is being driven via signalling from papillary cells to the papillary collecting ducts with Crim1 being critical for regulating the concentration and morphogen gradient of such a growth factor/s in this process. Recent studies suggest that Vegfa may be involved in growth of ureteric bud-derived epithelia via interaction with both the Vegfr2 (Flk1/Kdr) and directly with the Ret receptor, both of which are present in UB (Marlier et al 2009, Tufro et al 2007). It is therefore possible that Crim1 is again regulating Vegfa secretion, in this instance from the papillary interstitium and/or loops of Henle.

Crim1<sup>KST264/KST264</sup> mice display chronic renal disease characterized by interstitial fibrosis, inflammation, ~~renin recruitment~~ and vascular leakiness (Wilkinson et al, 2009). This is a progressive phenotype as it is not present in juvenile mice, although affected juveniles do show abnormal collagen deposition around the peritubular vasculature. As Crim1 is expressed in pericytes surrounding the renal vasculature, we had speculated that loss of Crim1 in these cells may be responsible for these extraglomerular renal defects (Wilkinson et al 2009). While, in part this may still be the case, our data show that functional obstruction is present in Crim1<sup>KST264/KST264</sup> mice even as juveniles. Based on previous studies of chronic obstruction (Chevalier 2009), this may be sufficient to explain all the extraglomerular features previously described in

these mice, including collagen deposition in juveniles, which may represent early evidence of interstitial fibrosis.

While it was initially proposed that progression to renal failure in CAKUT patients resulted from repetitive urinary tract infections associated with VUR or obstruction, it is now generally accepted that underlying renal dysplasia is more likely to be involved (Murer et al, 2007). A strong association exists between dysplasia upon postnatal renal ultrasound and poor long term renal function (Ismaili et al, 2006). What our study suggests is that minor anomalies of urinary tract development unlikely to be detected at birth may also contribute to renal disease in later life. The contribution of such minor anomalies to the burden of chronic renal disease in children or adults is unknown. These findings should prompt the nephrology community to consider papillary structure in renal disease patients as undetected defects in papillary development such as we have described here may contribute to the one third of cases of childhood CKD not specifically associated with diagnosed CAKUT. The nephrology community now embraces the ~~data showing an~~ association between reduced nephron number and onset of renal failure later in life (Brenner hypothesis). The results presented here raise the possibility of a similar link between reduced papillary length and ~~mild functional obstruction that may progressive to~~ chronic kidney disease.

### **Acknowledgements**

We acknowledge the support of the Queensland Government Smart State initiative for the 16.4T MRI scanner, which was provided through the Queensland NMR Network. We thank Joan Li for the surgery involved in generating the Supplementary data. We also thank the support of the staff of the School of Biomedical Sciences Animal Facility. YLP holds an Australian Postgraduate Scholarship. ML is an NHMRC Principal Research Fellow (511032).

## **Materials and Methods**

### **Mice**

Maintenance and production of mice carrying the KST264 transgene have been previously described (Wilkinson et al, 2009). All animal production and use was carried out in accordance with the certification of the animal ethics committee, University of Queensland (IMB/160/08/NHMRC). Genotyping was performed by PCR on tail tips taken at 10 days of age. Wild-type and *Crim1*<sup>KST264/KST264</sup> same sex siblings (8 pairs) were used for imaging experiments. Ages ranged from 4 wks to 8 months. Eight pairs of males and 2 pairs of females were used.

### **Histology and immunohistochemistry**

Harvested kidneys were bisected and fixed in 4% paraformaldehyde in phosphate buffered saline (PBS) for 24 hrs prior to processing and paraffin embedding, or for 30 minutes prior to cryopreservation. Paraffin sections were cut at 7 µm. Standard haematoxylin and eosin staining or eosin alone as a counter stain, and Masson's green trichrome staining was performed as described (Wilkinson et al 2007, 2009). Tissue for cryopreservation was equilibrated overnight in 30% sucrose, then 1:1 30% sucrose, optimal cutting temperature, then frozen in Tissue Tek ® O.C.T (Sakura-Finetek Europe B.V. The Netherlands) on dry ice. Sections were cut at 10 µm and dried overnight before immunostaining. Primary antibodies used were aquaporin 1 and aquaporin 2 (Millipore Australia, North Ryde, NSW, Australia). Secondary antibodies were anti-rabbit alexa-Fluor 488 (Invitrogen Australia Pty Ltd, Mulgrave, Victoria, Australia.) Detection of apoptotic nuclei was performed on cryosections using a TUNEL kit according to manufacturers protocol (Roche Diagnostics Australia Pty. Ltd.

Castle Hill, NSW, Australia).  $\beta$ -Galactosidase activity was visualised as previously described (Pennisi et al, 2007).

### **Rhodamine dextran treatment**

Tetramethylrhodamine dextran (10 kDa) (Invitrogen Australia Pty Ltd, Mulgrave, Victoria, Australia.) (100  $\mu$ l of 10 mg/ml in PBS) was injected via tail vein into two female *Crim1*<sup>KST264/KST264</sup> mice and one female wild-type mouse. Kidneys were harvested after 40 minutes, bisected for photography then cryopreserved.

### **Surgical Methods**

Animals were anaesthetised with 1.5-2% isoflurane. For unilateral ureteric obstruction, a flank incision was made to visualise the left ureter, which was then obstructed by tying with suture silk (Syneture 5-0 SOFSILK, Covidien, Dublin Ireland), as previously described (Cochrane et al 2005). For IRI, the left renal artery was visualised and was clamped (S&T B-1 vascular clamp 7mm, Fine Science Tools Inc. North Vancouver, Canada) for 50 minutes. After this time, the clamp was removed to allow reperfusion (Verghese E et al 2007). Mice underwent MR imaging after 24 hrs, and were sacrificed on completion of imaging and kidneys harvested.

### **MRI method for kidney imaging:**

MRI was performed on a 16.4T/89mm magnet with an Avance II NMR scanner and Paravision 5.0 software (Bruker Biospin, Ettlingen, Germany). It was equipped with Micro2.5 gradient and MicroMouse whole body animal probe system. During imaging the animal was anesthetized with 2% isoflurane at 1.5 L/min, and the respiration rate was monitored using BIOTRIG. The animals were kept warm using the gradient

cooling water circulation at 30 degrees. Contiguous 0.8 mm slices of entire kidneys were acquired. Image acquisition, and therefore resolution, was more problematic for Crim1<sup>KST264/KST264</sup> mice due to respiration irregularities.

### **Magnevist clearance study**

Gd-DTPA (Magnevist®, Bayer-Schering) is a negatively charged, gadolinium containing contrast agent which is used to show normal blood perfusion. The small molecular weight (<1kDa) and biochemical properties of Gd-DTPA enables rapid distribution throughout all tissues other than the central nervous system, where the blood brain barrier is impermeable to this molecule. The volume of distribution in the tissues is equivalent to that of extracellular water and in humans the distribution half-life is approximately 4 minutes (Abraham JL 2008). At a small concentration it will show hyperintensity (bright) under a T1-weighted images. However, at higher concentration (through accumulation) the shortening of T<sub>2</sub> effects becomes predominant, thus images will start to be show hypointensity (dark). For the clearance study, Gd-DTPA 0.1-0.15 mmol/kg body weight was administered as tail vein bolus injection. T1-weighted images were acquired using a multislice spin echo (MSME Bruker) sequence. The MRI parameters were TR/TE = 500/11 ms, NEX=4, 117 x 117 µm in-plane spatial resolution, 0.8 mm contiguous slices. The imaging time was 8 mins. An image baseline was acquired before the administration of the contrast agent, immediately upon administration and then serially for approximately 2 hours.

### **Image analysis**

MRI data was exported as DICOM files and analyzed using the software Osirix Imaging Software (Rosset A et al (Journal of Digital imaging). Following 3D Fourier transform,

the MRA data was projected onto a single image using maximum intensity projection. Measurements including signal intensity were determined using a manual region of interest segmentation.

### **Movies of pyeloureteric peristalsis**

Peristalsis was recorded as previously described (Hurtado et al, 2010) with minor modifications. In brief, whole adult kidneys with the ureter attached were isolated from wild-type and *Crim1<sup>KST264/KST264</sup>* mice and placed into prewarmed DMEM/F12 media. Excessive tissue surrounding the kidney and ureter was carefully removed using a pair of fine forceps. To expose the renal papilla, pelvis and ureter, kidneys were dissected longitudinally using a no. 10 scalpel blade under a dissecting microscope. Bisected kidneys were placed into Nunc 6 well dishes in 800µl prewarmed DMEM/F12 media and incubated for at least 10 minutes at 37°C, 5% CO<sub>2</sub>. [Analysis was performed on a total of 10 non-mutant and 8 kidneys from 3-12 weeks of age.](#) Peristaltic contractions were recorded using a DP-70 12Mp Colour camera attached to an Olympus SZX-12 stereo dissecting microscope. The Olympus DP controller software generated a 3 minute MPEG-1 680 X 512 movie file. Contraction frequency was plotted from raw data by visually noting the timing of contractions at two adjacent points; the origin of contraction around the base of the papilla (A) and the ureter at the tip of the papilla (B), as well as the time at which the tip of the papilla returned to the position of precontraction (B'). Videos were processed using the edge detection component of ImageJ and spatial temporal maps created with Andor IQ software. Constrictions were expressed as a percentage reduction of the tissue diameter at each point of interest, propagation velocity calculated from the interval and distance between constrictions between two points of interest.

### **Quantitation and Statistical Analysis**

Statistical analysis was performed using Prism 5 (GraphPad Software Inc., La Jolla, CA, USA). Significance was determined by Student's t-test.

### **Electrophysiological studies**

Whole kidneys with the ureter attached were isolated, cleared of surrounding tissue, bisected caudally to expose the papilla, renal pelvis and ureter and placed into a 6 well dish in prewarmed DMEM/F12 media. Kidneys were imaged (at 24 frames  $s^{-1}$ ) for 10 minutes using a stereo Olympus SZX-12 dissecting microscope with a DP-70 12Mp Colour camera. One minute of typical activity was processed for peristaltic activity using edge detection software (ImageJ)(Fig Aii,Bii)

In the organ bath experiments, the renal pelvis and proximal ureter were dissected completely free of the papilla and surrounding tissue and pinned into an organ bathed, which was perfused with a physiological salt solution (PSS) (37°C) at 2-3  $ml\ min^{-1}$ . The bath was placed on a dissection microscope (Nikon SMZ1000), images of propagating contractions were captured digitally (at 25 frames  $s^{-1}$ ) onto a computer as well as onto an analog video tape for later analysis.

Spatial temporal maps of the movement of the renal pelvis attached to or dissected free of the papilla were created at 2-3 points of known separation along the muscle wall. Aligning these maps in time allowed the calculation of both the frequency and velocity of the spontaneous contractions in the renal pelvis under both *in vitro* experimental conditions. The action of applied agents was also established by

monitoring changes in organ diameter at the one point along the renal pelvis using Diamtrak software.

### **Calcium imaging**

Renal pelvis dissected from the papilla, opened up longitudinally and pinned flat in an organ bath were loaded with fluo-4AM as previously described (Lang et al 2007a,b). Preparations were incubated in low  $\text{Ca}^{2+}$  physiological salt solution (PSS) ( $[\text{Ca}^{2+}]_o = 0.5 \text{ mM}$ ) containing  $10 \mu\text{M}$  fluo-4 AM (special packaging, Invitrogen) and cremphor EL (0.01 %, Sigma) for 30 min at  $36 \text{ }^\circ\text{C}$ . Following incubation, tissue preparations were superfused with dye-free, warmed ( $36 \text{ }^\circ\text{C}$ ) normal  $\text{Ca}^{2+}$  PSS ( $[\text{Ca}^{2+}] = 2.5 \text{ mM}$ ) and illuminated at 495 nm fluorescence,  $\text{Ca}^{2+}$  signal emissions (above 515 nm) were detected and captured for later analysis using Andor iQ software (© 2011 Andor Technology plc.). Relative changes in intracellular  $\text{Ca}^{2+}$  were expressed as the ratio ( $F_t / F_o$ ) of the fluorescence generated by an event ( $F_t$ ) against baseline ( $F_o$ ).

The physiological salt solution (PSS) contained (in mM): NaCl 120, KCl 4.7,  $\text{CaCl}_2$  2.5,  $\text{MgCl}_2$  1.2,  $\text{NaHCO}_3$  15.5,  $\text{KH}_2\text{PO}_4$  1.2 and glucose 15. The pH of this PSS was 7.2 when bubbled with 95%  $\text{O}_2$  and 5%  $\text{CO}_2$ . Drugs used were dinoprost, indomethacin, phenylephrine, nifedipine (from Sigma, St Louis, MO, USA). Phenylephrine, indomethacin and dinoprost were dissolved in PSS as a stock solution (0.1-10 mM), while nifedipine was dissolved in absolute ethanol. The final concentration of these solvents in the PSS did not exceed 1 : 1000.

### **Data Analysis for contractile studies**

Mean  $\pm$  standard deviation of the mean (mean  $\pm$  S.D.) are presented with n denoting the number of observations. Paired or unpaired Student's t-tests were used for tests of significance;  $p < 0.05$  was accepted as statistically significant

**Stuff still to be added:**

LacZ staining for neonatal pelvis development data – could be added to histology section

Measurement of papillary extrusion and statistics applied

### **Acknowledgements**

We acknowledge the support of the Queensland Government Smart State initiative for the 16.4T MRI scanner, which was provided through the Queensland NMR Network.

We also thank the support of the staff of the School of Biomedical Sciences Animal Facility. YLP holds an Australian Postgraduate Scholarship. ML is an NHMRC Principal Research Fellow (511032).

## References

1. Winyard P, Chitty LS. Dysplastic kidneys. (2008) *Semin Fetal Neonatal Med.* 13(3):142-51.
2. Schedl A. Renal abnormalities and their developmental origin. (2007) *Nat Rev Genet.* 8(10):791-802.
3. Klein
4. Lang?
5. Lang?
6. Gosling JA, Dixon JS. Species variation in the location of upper urinary tract pacemaker cells. *Invest Urol* 1974; 11: 418–423.
7. Lang 2010
8. Dwyer TM, Schmidt-Nielsen B. The renal pelvis: machinery that concentrates urine in the papilla. (2003) *News Physiol Sci.* 18:1-6
9. Wilkinson 2007
10. Wilkinson 2009
11. Wilkinson, L., Kolle, G., Wen, D., Piper, M., Scott, J. and **Little M.H.** CRIM1 regulates the rate of processing and delivery of BMPs to the cell surface. (2003) *J. Biol. Chem* 278(36):34181-8
12. Grenier 2009
13. Abraham JL 2008
14. Choyke et al, 2005
15. Cochrane et al, 2005
16. Verghese E et al 2007
17. Chevalier R 2009
18. Sutton et al 2003
19. Hurtado
20. Pennisi et al, 2007
21. HH in smooth muscle
22. RAS in smooth muscle
23. Bmp4 in smooth muscle
24. Chang 2004
25. Proliferation in collecting ducts
26. Yu
27. Karner
28. Pietela
29. Suburi
30. EGF

31. RAS
32. Marlier A, Schmidt-Ott KM, Gallagher AR, Barasch J, Karihaloo A. VEGF as an epithelial cell morphogen modulates branching morphogenesis of embryonic kidney by directly acting on the ureteric bud. (2009) *Mech Dev.* 126(3-4):91-8
33. Tufro A, Teichman J, Banu N, Villegas G. Crosstalk between VEGF-A/VEGFR2 and GDNF/RET signaling pathways. (2007) *Biochem Biophys Res Commun.* 358;410-416
34. Murer
35. Ismaili
36. Brenner

Klein J, Gonzalez J, Miravete M, Caubet C, Chaaya R, Decramer S, Bandon F, Bascands J-L, Buffin-Meyer B, Schanstra JP. Congenital ureteropelvic junction obstruction: human disease and animal models.

Truong LD, Gaber L, Eknayan G. Obstructive uropathy. *Contrib Nephrol.* 2011;169:311-26.

Thornhill BA, Burt LE, Chen C, Forbes MS, Chevalier RL. Variable chronic partial ureteral obstruction in the neonatal rat: a new model of ureteropelvic junction obstruction. (2005) *Kidney Int.* 67(1):42-52.

Wong A, Bogni S, Kokta P, de Graaff E, D'Agati V, Costantini F, Pachnis V. Phosphotyrosine 1062 is critical for the in vivo activity of the Ret9 receptor tyrosine kinase isoform. (2005) *Mol. Cell Biol.* 25:9661-73

Hoshino T, Shimizu R, Ohmori S, Nagano M, Pan X, Ohneda O, Khandekar M, Yamamoto M, Lim KC, Engel JD. Reduced BMP4 abundance in *Gata2* hypomorphic mutant mice result in uropathies resembling human CAKUT (2008) *Genes Cells.* 13(2):159-70.

Constantinou CE, Yamaguchi O. Multiple-coupled pacemaker system in renal pelvis of the unicalyceal kidney. *Am J Physiol* 1981; 241: R412-R418.

Lang RJ, Hashitani H, Tonta MA *et al.* Spontaneous electrical and Ca<sup>2+</sup> signals in typical and atypical smooth muscle cells and interstitial cell of Cajal-like cells of mouse renal pelvis. *J Physiol* 2007; 583: 1049–1068.

Lang RJ. Role of hyperpolarization-activated cation channels in pyeloureteric peristalsis. *Kidney Int.* 2010 Mar;77(6):483-5.

Lang RJ, Hashitani H, Tonta MA, Bourke JL, Parkington HC, Suzuki H. Spontaneous electrical and Ca<sup>2+</sup> signals in the mouse renal pelvis that drive pyeloureteric peristalsis. *Clin Exp Pharmacol Physiol.* 2010 Apr;37(4):509-15.

### Figure legends:

#### **Figure 1: MRI reveals extensive cortical cysts and a loss of CMD in**

***CrimI*<sup>KST264/KST264</sup> mice.** Anatomical scans using T<sub>2</sub> weighted RARE sequence were performed on wild-type (A) and *CrimI*<sup>KST264/KST264</sup> mice (C) mice. Contiguous slices through the wild-type kidney show a clear distinction between cortex, medulla and papilla. (A). The central slice of a wild-type kidney with a hemimount of the same kidney showing correlation is shown with the MRI scan and visible compartments marked (B). The *CrimI*<sup>KST264/KST264</sup> kidney (C) shows numerous cysts and diminishing CMD. The central slice of HZ7-L (D) shows a complete loss of CMD, a large cyst and hydronephrosis. The hemimount of the same kidney shows the dilated pelvis and atrophied papilla indicating hydronephrosis as well as the large cyst. C, cortex; M, medulla; P, papilla.

**Comment [m1]:** I would remove this Figure and start the story with the histological quantitation of hydronephrosis

#### **Figure 2. Adult *CrimI*<sup>KST264/KST264</sup> mice show evidence of progressive**

**hydronephrosis.** Anatomical scans using T<sub>2</sub> weighted RARE sequence of a *CrimI*<sup>KST264/KST264</sup> mouse at ages 11, 16 and 37 wks shows presence of hydronephrosis at 37 wks only. Representative trichrome stained mid-section through age matched wild-type (A) and hydronephrotic *CrimI*<sup>KST264/KST264</sup> kidney (B) showing multiple glomerular cysts, atrophied papilla and dilated pelvis. Tunnel staining identifies apoptotic cells lining the renal pelvis in *CrimI*<sup>KST264/KST264</sup> kidney (C).

#### **Figure 3. Dynamic contrast enhanced MRI shows accumulation of Gd-DTPA in**

**the *CrimI*<sup>KST264/KST264</sup> kidney.** T1 weighted images were obtained prior to and approximately every 10 minutes after Gd-DTPA injection in both wild-type and

*Crim1*<sup>KST264/KST264</sup> mice for up to 3.5 hours. In the wild-type kidney Gd-DTPA rapidly spread throughout the kidney but was concentrated in the papilla, indicated by hypointensity of Gd-DTPA, as it is concentrated and excreted in the urine. Gd-DTPA is rapidly cleared and by 211 minutes kidney intensity has returned to baseline (A, C). In contrast in the *Crim1*<sup>KST264/KST264</sup> kidney Gd-DTPA accumulated throughout the kidney, shown by increasing hypointensity. Even after 19 hrs the Gd-DTPA intensity had not returned to baseline (B, C). Intensities of wild-type and *Crim1*<sup>KST264/KST264</sup> are shown graphically (C).

~~**Figure 4. Surgical models of renal damage confirm Gd-DTPA accumulation is due to obstruction.** Ischemia reperfusion injury (A) and unilateral ureteral obstruction (B) was performed on the left kidney of two wild-type CD1 mice. The right contraateral kidney acted as an internal control. DCE MRI was performed on both mice as well as anatomical scans. Mice were euthanased on completion of the scans and kidneys were removed. Hemimounts are shown. Contralateral kidneys in both models are comparable to control mice, while the IRI kidney shows a loss of concentrating ability of Gd-DTPA in the papilla and the UUO kidney shows accumulation of Gd-DTPA throughout the kidney. The T<sub>2</sub> scan and hemimount of the IRI kidney shows vascular haemorrhage in the medulla (arrows), while that of the UUO kidney shows hydronephrosis (\*).~~

**Figure 54. Accumulation of tubular rhodamine dextran indicates outflow obstruction.** Rhodamine Dextran (10kDa) was injected via tail vein into wild-type and *Crim1*<sup>KST264/KST264</sup> mice and mice were euthanized after 40 minutes. The control kidney (A) showed little autofluorescence. RD remained only in the papilla of the wild-type kidney (B), while RD was seen throughout the kidneys of two *Crim1*<sup>KST264/KST264</sup> mice

(C,D). Particularly bright spots were evident in the *Crim1*<sup>KST264/KST264</sup> kidneys (C,D arrows). Aquaporin 1 (E,F) and aquaporin 2 (G,H) immunofluorescence of cryosections of *Crim1*<sup>KST264/KST264</sup> kidneys overlaid with RD fluorescence showed RD accumulation in collecting ducts in cortex (G) and predominantly papilla (H).

**Figure 56. Characterization of peristalsis in hemidissected *Crim1*<sup>+/+</sup>, *Crim1*<sup>KST264/+</sup> and *Crim1*<sup>KST264/KST264</sup> kidneys.** Videos (1.5 min) of spontaneous contractions in 3 week old wild type (Ai) and *Crim1*<sup>KST264/KST264</sup> (Bi) renal pelvis were processed using edge detection software. Temporal mapping of peristaltic contractions at points a and b are coordinately displayed below (Aii, Bii). While contractions propagate distally along the pelvis and ureter in the *Crim1*<sup>+/+</sup> mice (shown by slope of dotted line in Aii, contractions were more usually synchronous in the *Crim1*<sup>KST264/KST264</sup> kidneys. No significant difference in peristaltic frequency was observed between the two groups, (wild-type  $7.8 \pm 0.99 \text{ min}^{-1}$  (mean  $\pm$  S.E.M); mutant  $5.95 \pm 0.99 \text{ min}^{-1}$ ,  $P > 0.05$ ).

Formatted: Font color: Auto

Formatted: Font color: Auto

**Figure 67. Assessment of the contractile properties of the pelvic smooth muscle in wildtype and *Crim1* mutant kidneys.** Isolated renal pelvis from all three genotypes were analysed for contractile properties. A. Transient increases in  $\text{Ca}^{2+}$  were seen to propagate across the field of view (yellow arrows) in sequential  $\text{Ca}^{2+}$  fluorescent micrographs (100 ms apart) of fluo-4 loaded smooth muscle cells of both wild-type (WT) (Ai) and *Crim1*<sup>KST264/KST264</sup> homozygous (HOM) mice (Aii).  $\text{Ca}^{2+}$  transients occurred almost simultaneously along the length of individual smooth muscles and propagated along the longitudinal axis of the renal pelvis, perpendicular to the mostly

circumferentially orientated smooth muscle cells. The amplitude and frequency of  $\text{Ca}^{2+}$  waves was not significantly different between the two groups (non-mutant: mean amplitude  $0.47 \pm 0.2 F_t / F_0$  and frequency  $12.8 \pm 6.3 \text{ min}^{-1}$ , n=5 from 3 animals; mutant:  $0.3 \pm 0.29 F_t / F_0$  and frequency  $17.5 \pm 11.9 \text{ min}^{-1}$ , n=4 from 3 animals).  $\text{Ca}^{2+}$  waves and their associated contractions were blocked in all animals upon the application of the L-type Ca channel blocker, nifedipine (1  $\mu\text{M}$ ) (not shown). **Scale bar:**

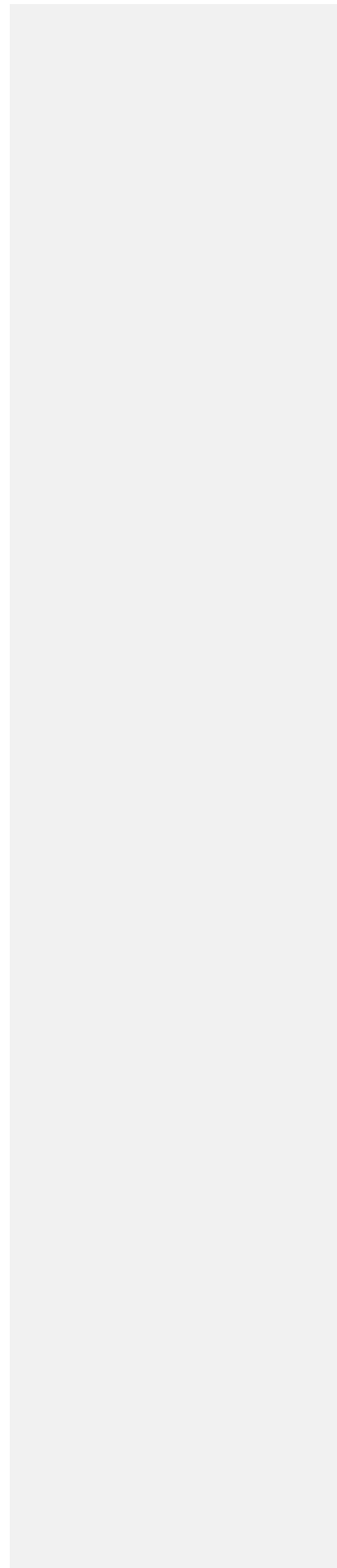
**Comment [112]:** What are the values for WT?

\*\*\*\*. B/C. WT (B) and Hom (C) mice responded similarly to High  $\text{K}^+$  levels (30 mM) which decreased the frequency of spontaneous constrictions of the mid renal pelvis (Bi, Ci). Downward deflections represent constrictions expressed as a percentage of the relaxed diameter of the tissue. The basal tone and frequency of the spontaneous contractions of WT (Bii) and Hom (Cii) mice were reduced upon blockade of prostaglandin synthesis with indomethacin (10 and 20 mM for 10-30 min). Constriction frequency in the presence of indomethacin (20 mM) was readily restored to baseline levels in the presence of Dinoprost, the stable analog of prostaglandin  $\text{F}_{2\alpha}$  [mice (Biii, Ciii). Frequency (Di) and velocity (Dii) of contractions are shown graphically for both WT and Hom mice. \*,  $p < 0.05$

**Figure 78.  $\text{Crim1}^{\text{KST264/KST264}}$  mice show papillary hypoplasia.** AB. Photographs of whole neonatal kidneys from wild-type (A) and  $\text{Crim1}^{\text{KST264/KST264}}$  (B) kidneys illustrating the lack of papillary protrusion in  $\text{Crim1}^{\text{KST264/KST264}}$  mice. C. Plot of papilla length as a proportion of kidney length from birth (P0) to P15 in wild-type and  $\text{Crim1}^{\text{KST264/KST264}}$  mice. D-\*\*. B-galactosidase staining of sections from wild-type,  $\text{Crim1}^{+/KST264}$  and  $\text{Crim1}^{\text{KST264/KST264}}$  kidneys showing expression of  $\text{Crim1}$ . LacZ staining was detected in the very tip of the P0 papilla, becoming more widespread as

elongation occurs. Cell types expressing Crim1 in the developing papilla include interstitium and Loop of Henle but exclude medullary collecting duct epithelium (E).

|



## -Supplementary data

### Gd-DTPA accumulation is seen in unilateral ureteric obstruction.

To confirm Gd-DTPA accumulation and concentration in the kidney occurred as a result of reduced urinary filtrate clearance rather than the leaky peritubular vasculature previously reported in this genotype,<sup>S1</sup> DCE MRI was performed on wild-type mice subjected to either unilateral ureteral obstruction (UUO) for 24 hours<sup>S2</sup> or unilateral renal ischemia due to 50 minutes of renal artery clamping followed by reperfusion (IRI).<sup>S3</sup> The contralateral kidney in both these models acted as an internal control and all kidneys were imaged 24 hrs after surgery. Quantitation of Magnevist clearance is shown in Supplementary Figure 1C. Renal damage after 24 hrs UUO is limited to mild hydronephrosis, reduced renal blood flow and GFR,<sup>S4</sup> while injury at 24hrs post IRI results in leaky peritubular vasculature, interstitial inflammation and edema.<sup>S5</sup> Hemimounts of kidneys were harvested immediately after imaging. Mild hydronephrosis / pelvic dilation was evident in the UUO kidney (Supplementary Figure 1C). Hemorrhagic congestion apparent in the medulla of the IRI kidney (Supplementary Figure 1A) is typical of hypoxic injury to the medulla and is associated with localised decreases in MRI signal intensity due to the paramagnetic characteristics of the iron within the hemoglobin.<sup>S6</sup> DCE imaging of the contralateral kidneys for both damage models showed results consistent with a normal kidney. While hypointensity did not occur in any region of the IRI kidney (Supplementary Figure 1A), hypointensity was evident throughout the UUO kidney within 30 minutes of Magnevist injection and remained for the duration of imaging (Supplementary Figure 1B). Hence, obstruction does indeed result in widespread hypointense staining.

Formatted: Superscript

**Supplementary Figure 1. Surgical models of renal damage confirm Gd-DTPA accumulation is due to obstruction.** Ischemia reperfusion injury (A) and unilateral ureteral obstruction (B) was performed on the left kidney of two wild-type CD1 mice. The right contraateral kidney acted as an internal control. DCE MRI was performed on both mice as well as anatomical scans. Mice were euthanased on completion of the scans and kidneys were removed. Hemimounts are shown. Contralateral kidneys in both models are comparable to control mice, while the IRI kidney shows a loss of concentrating ability of Gd-DTPA in the papilla and the UO kidney shows accumulation of Gd-DTPA throughout the kidney. The T<sub>2</sub> scan and hemimount of the IRI kidney shows vascular haemorrhage in the medulla (arrows), while that of the UO kidney shows hydronephrosis (\*).

#### **Supplementary Movie 1**

Formatted: Font: Bold

#### **Supplementary Movie 2**

#### **Supplementary Movie 3**

#### **Supplementary Movie 4**

#### **Supplementary References**

S1. Wilkinson et al, 2009

Formatted: Normal, Line spacing: Double, No bullets or numbering

S2. Cochrane et al, 2005

Formatted: Font: Times New Roman

S3. Verghese E et al 2007

Formatted: Font: Times New Roman

S4. Chevalier R 2009

Formatted: Font: Times New Roman

S5. Sutton et al 2003

Formatted: Normal, Justified, Line spacing: Double, No bullets or numbering

S6. Grenier 2009

Formatted: Font: Times New Roman